Quantifying the impact of COVID-19 non-pharmaceutical interventions on influenza transmission in the United States

Yuchen Qi[1], Jeffrey Shaman[2], Sen Pei[*,2]

[1]Department of Biostatistics, Mailman School of Public Health, Columbia University, New York, NY 10032, USA

[2]Department of Environmental Health Sciences, Mailman School of Public Health, Columbia University, New York, NY 10032, USA

[*]Correspondence to: S.P. (sp3449@cumc.columbia.edu)

Summary: Incidence of influenza A/H1 and B were reduced by more than 60% in the US during the first ten weeks following implementation of NPIs. Potential large outbreaks of influenza may occur after the relaxation of NPIs.

Conflict of Interest

JS and Columbia University disclose partial ownership of SK Analytics. JS discloses consulting for BNI. Other authors declare no conflict of interest.

Funding

This work was supported by the National Science Foundation (DMS-2027369 to J. S.) and a gift from the Morris-Singer Foundation (to J. S.).

Corresponding author

Sen Pei

722 W 168th St, Room 1104A, New York, NY 10032

E-mail: sp3449@cumc.columbia.edu

Abstract

Background: Nonpharmaceutical interventions (NPIs) have been implemented to suppress the transmission of severe acute respiratory syndrome coronavirus 2 (SARS-CoV-2). Evidence indicates that NPIs against COVID-19 may also have effects on the transmission of seasonal influenza.

Methods: In this study, we use an absolute humidity-driven susceptible-infectious-recovered-susceptible (SIRS) model to quantify the reduction of influenza incidence and transmission in the US and HHS (the US Department of Health and Human Services) regions after implementation of NPIs in 2020. We investigate the long-term effect of NPIs on influenza incidence by projecting influenza transmission at the national scale over the next five years, using the SIRS model.

Results: We estimate that incidence of influenza A/H1 and B, which circulated in early 2020, was reduced by more than 60% in the US during the first ten weeks following implementation of NPIs. The reduction of influenza transmission exhibits clear geographical variation. After the control measures are relaxed, potential accumulation of susceptibility to influenza infection may lead to a large outbreak, the scale of which may be affected by length of the intervention period and duration of immunity to influenza.

Discussion: Healthcare systems need to prepare for potential influenza patient surges and advocate vaccination and continued precautions.

Key words: Non-pharmaceutical interventions; COVID-19; SARS-CoV-2; Influenza; Influenza forecasting

Backgrounds

Since December 2019, the spread of severe acute respiratory syndrome coronavirus 2 (SARS-CoV-2) has caused more than one hundred fifty million confirmed cases globally as of May 2021, including more than thirty million confirmed infections in the US [1-3]. To suppress the COVID-19 pandemic, non-pharmaceutical interventions (NPIs) have been implemented worldwide, including travel restrictions, face masks, social distancing, public education on prevention measures, and school closures [4-8]. These control measures have not only disrupted the spread of COVID-19, but also modulated the transmission of other pathogens such as influenza [9-14], respiratory syncytial virus [9], dengue virus [15,16] and enterovirus [17].

Seasonal influenza causes an enormous health and economic burden in the US, including substantial morbidity and mortality, as well as direct medical costs and indirect costs due to illness and loss of life every year [18]. Influenza virus shares the same putative transmission pathways of SARS-CoV-2 [19-21]. It is therefore reasonable to postulate that NPIs against COVID-19 may have reduced influenza transmission as well. Studies have reported a substantial decline in influenza transmission after the implementation of NPIs in Hong Kong and mainland China [10, 11]. For instance, the incidence rate of influenza during the 2019-2020 season was reduced by 64% compared with the previous two seasons in China. In the US, a similar earlier decrease of influenza-like illness (ILI) during spring 2020 compared to prior seasons was also reported [9, 12].

Although evidence indicates that control measures against COVID-19 have reduced the transmission of seasonal influenza, accurate quantification of the reduction of influenza incidence in the US has remained challenging. Influenza activity exhibits large variations in peak timing and intensity across seasons (Fig. 1); as a result, using historical averages to

estimate reductions of influenza incidence is not reliable. In addition, as multiple types/subtypes of influenza co-circulate in a given population with variable seasonal phasing, it is necessary to compute the reduction for each type/subtype rather than the aggregated influenza signal. Further, variations in regional influenza dynamics and the implementation of NPIs could potentially lead to pronounced geographical differences of incidence reduction, which cannot be captured in a national-level analysis.

In this study, we address these challenges by developing a climate-forced influenza transmission model that is applied to each type/subtype of influenza circulating in the US and 10 HHS (the US Department of Health and Human Services, see Supplementary Figure 1 for the HHS regional map) regions during early 2020. We use this model to generate predictions for influenza A/H1 and B after March 15, 2020, when NPIs in most states started, and estimate the percentage reduction of incidence for each type/subtype in each region. We further explore the long-term effect of NPIs on influenza incidence by projecting transmission dynamics over the next five years under various control scenarios.

Methods

Data

We used data from the CDC FluView website to track influenza activity in the US [22]. It contains weekly percentages of patient visits for ILI in the US and 10 HHS regions since the 1997-1998 season (Figure 1A). Weekly positivity rates for influenza subtypes A/H1 and B, derived from laboratory testing, are also available for the US and each region. As ILI is not exclusively attributed to influenza, we multiply weekly ILI by its concurrent positivity rate for influenza A/H1 (or B) to represent influenza activity. We use the composite signal, termed ILI+, to represent the percentage of patient visits due to influenza A/H1 or B (Figure 1B-C) [23]. For computational convenience, we transformed the unit of ILI+ from percent to

incidence per 100,000 people. Evidence suggests that the transmission of influenza is modulated by local absolute humidity (AH) conditions [24]. AH conditions in the US and 10 HHS regions were taken from daily climatological humidity data averaged over a 24-y period (1979–2002) derived from North American Land Data Assimilation System data [25].

Humidity-forced SIRS model

The model used for this study is an absolute humidity-driven susceptible-infectious-recovered-susceptible (SIRS) model [26-29]. The equations for the SIRS model are:

$$\frac{dS}{dt} = \frac{N - S - I}{L} - \frac{\beta(t) I S}{N}$$

$$\frac{dI}{dt} = \frac{\beta(t) I S}{N} - \frac{I}{D}$$

where S is the number of susceptible people in the population, N is the population size, I is the number of infectious people, N-S-I is the number of recovered individuals, L is the average duration of immunity, D is the mean infectious period, and $\beta(t)$ is the contact rate at time t. New incidence is computed from the transmission term $\beta(t)IS/N$.

The contact rate $\beta(t)$ is determined by the equation $\beta(t) = R_0(t)/D$. Here the basic reproduction number $R_0(t)$ is the average number of secondary infections that an infectious person would produce in a fully susceptible population at time t. This term is modulated through $R_0(t) = R_{0min} + (R_{0max} - R_{0min})e^{-aq(t)}$ [30], where R_{0max} is the maximum daily basic reproductive number, and R_{0min} is minimum daily basic reproductive number, q(t) is time-varying daily specific humidity, a measure of AH, and a is derived from the laboratory experiments documenting influenza virus survival under different AH conditions and is set to 180 [24]. We estimated the parameters R_{0max}, R_{0min}, the mean infectious period D, and the

mean duration of immunity L using a Markov Chain Monte Carlo method, described in following subsections.

Estimates of influenza incidence in the general population

ILI+ measures the percentage of patient visits attributed to influenza. To match this observation in healthcare systems to influenza incidence in the general population, we linked ILI+ to population-level influenza prevalence using the relationship $p = \gamma\ ILI +$, where p is the fraction of the population newly infected with influenza in a given week. This relationship is derived using the Bayes rule [23], and the scaling parameter γ is the ratio of the probability that a person seeks medical attention for any reason to the probability that a person with influenza seeks medical attention. For computational convenience, we used weekly new incidence per 100,000 people, $I_{new} = p \times 10^5$, as the observational unit. The scaling parameter γ is fixed for each season but is allowed to vary in different years due to changing healthcare-seeking behavior [23]. In retrospective forecasts, we generated predictions using different values of γ and found that $\gamma =$ 2.5 yields satisfactory predictive skill for most seasons. For the 2019-2020 season, the ILI+ observations are much higher than preceding years and $\gamma =$ 1 was used to infer reasonable parameter estimates with the SIRS model.

Model calibration using MCMC

Parameters of the SIRS model were estimated using a Markov chain Monte Carlo (MCMC) method. Specifically, we calibrated the model to observed weekly new incidence per 100,000 people, I_{new}. We assumed weekly new incidence follows a negative binomial distribution with a mean equal to observed I_{new} and a dispersion of h, where the unknown parameter h is fixed for all observations. The variance is $I_{new} + I_{new}^2/h$ in this parametrization. We employed MCMC to estimate the following parameters: $[R_{0max}, R_{0min}, D, L, h, S_0, I_0]$. A

component-wise Metropolis-Hastings algorithm was adopted to infer the multivariate distribution of the parameters [31]. Initial priors were set as uniform distributions in the following ranges: $0.8 \leq R_{0min} \leq 4$, $0.8 \leq R_{0max} \leq 4$, $2 \leq L \leq 10$ (years), $2 \leq D \leq 10$ (days), $1 \leq h \leq 1000$. In each step, a sequence of proposals for the five parameters and two initial conditions were generated and each proposal accepted or rejected in turn based on the likelihood of observing the entire time series. Specifically, the proposal was always accepted if $\mathcal{L}_{prop} \geq \mathcal{L}_{cnt}$, and accepted with a probability $\mathcal{L}_{prop}/\mathcal{L}_{cnt}$ if $\mathcal{L}_{prop} < \mathcal{L}_{cnt}$, where $\mathcal{L}_{prop}$ and $\mathcal{L}_{cnt}$ are the likelihoods corresponding to the proposal and current parameter combinations. The likelihood is calculated using the assumed negative binomial distribution for the observations. The proposed value follows a uniform distribution centered at the current value. We discarded the first 8000 steps as burn-in and used the final 2000 steps to estimate the posterior parameter distributions. Following this MCMC approach, the posterior parameter distributions center around the maximum likelihood estimates in the parameter space, with uncertain quantified by the spread of distributions.

Retrospective forecasts

Accurate influenza forecasting is challenging due to the substantial cross-season variability of influenza incidence. Given such pronounced year-to-year differences (Fig. 1), a process-based model is appealing as it could potentially capture these shifting transmission dynamics. Here we coupled the humidity-forced SIRS model and MCMC to generate retrospective forecasts. Specifically, we calibrated the model to observations up to a given week, then integrated the model into the future using the estimated mean parameter values. Prediction uncertainty was generated using the negative binominal distribution.

We generated retrospective forecasts for influenza A/H1 and B in the seasons during which each type/subtype widely circulated in the population: A/H1: 2013-2014, 2015-2016, 2017-

2018, 2018-2019; B: 2012-2013, 2014-2015, 2015-2016, 2017-2018. Seasons with low incidence of A/H1 and B were omitted. We did not predict A/H3 as it was not prevalent during the 2019-2020 season. For those seasons, weekly forecasts were generated for the US and 10 HHS regions from the 20^{th} to the 25^{th} week in each season (influenza season starts from week 41 in each year, per the CDC definition on the FluView website [32]), matching the timing of the announcement of NPIs in the US during early 2020 (March 15, 2020 is during the 24^{th} week of season 2019-2020). Observations from the first week with incidence > 50 per 100,000 people to the forecast week were used to calibrate model parameters. In all the examined seasons, the first week with incidence > 50 per 100,000 people is after week 40 of that year, i.e., the beginning of influenza season. At each forecast week, predictions were generated until the end of season. Example forecasts for A/H1and B (Fig. 2) indicate that these predictions match observed incidence. To formally assess the performance of the SIRS-MCMC system, we performed retrospective forecasts using a baseline method, an autoregressive integrated moving average (ARIMA) model. We fit this ARIMA model using the function auto.arima from the R package "forecast" [33], which searches within the order constraints provided and gives the optimal estimation of parameters according to the AIC value.

Retrospective forecast evaluation

We evaluated forecast performance using two metrics: mean absolute error (MAE) and logarithmic score. MAE, designed to assess point predictions, quantifies the distance between average predictions and observed targets. Logarithmic score is calculated as the logarithm (base e) of the probability of forecasts assigned to a $\pm 10\%$ interval around the observed target and is a strictly proper scoring rule used to evaluate the accuracy of probabilistic forecasts. A floor value of -10 was set as a lower bound for logarithmic scores to address

probabilities close to zero. We computed MAE and logarithmic score for all predicted weeks (i.e., from the forecast week to the end of season).

Results

Example forecasts for A/H1and B (Fig. 2) indicate that these predictions match observed incidence. More forecast examples are provided in Supplementary Figures 2-3. Comparison between the SIRS-MCMC and ARIMA predictions (Supplementary Figure 4) demonstrates that the process-based model has a superior predictive skill with lower MAEs and higher logarithmic scores for both influenza A/H1 and B. The better performance of the SIRS-MCMC prediction is consistent across all forecast weeks. This retrospective forecast experiment validates that the process-based model can reliably predict the activity of influenza A/H1 and B in previous seasons during the period close to the NPI implementation during 2020.

Impact of NPIs on influenza incidence and transmission in 2020

To estimate counterfactual influenza transmission without NPIs against COVID-19, we generated predictions of influenza A/H1 and B beginning from the week of March 15, 2020 (the 24th week in the 2019-2020 season) for the US and 10 HHS regions. Figure 3 shows the fitted and predicted curves for influenza A/H1 and B at the national level, as well as observed incidence. Significant differences between expected and reported incidence are observed for both influenza types/subtypes. However, as influenza B peaked unusually early in 2019 winter, the NPIs have a more significant impact on influenza A/H1. Nationally, throughout the 2019-2020 season, the total incidence of influenza A/H1 was reduced 12.9% (95% CI, 10.9% - 15.0%), whereas influenza B was only reduced 4.7% (95% CI, 4.0% - 5.5%).

After March 15 2020, we define the reduction rate for a given week t as $\left|I_{new}^{pred}(t) - I_{new}^{obs}(t)\right|/I_{new}^{pred}(t)$, where $I_{new}^{pred}(t)$ and $I_{new}^{obs}(t)$ are the expected and observed new incidence in week t, respectively. For both influenza A/H1 and B, the national weekly incidence rapidly declined after the implementation of NPIs (Supplementary Table 1). A/H1 incidence is estimated to have been reduced by 61.8% (53.9% - 67.9%) during the first four weeks following NPIs, and 70.8% (66.7% - 74.3%) during the first ten weeks. For influenza B, incidence is estimated to have been reduced by 58.0% (49.4% - 64.6%) during the first four weeks and 67.4% (65.0% - 72.9%) during the first ten weeks following implementation of NPIs.

The reduction of influenza incidence exhibits clear geographical variation (Figure 4). For influenza A/H1, the averted incidence during the first ten weeks following enforcement of NPIs ranges from 68% to 88% across the 10 HHS regions, with the exception of region 2 (New Jersey, New York, Puerto Rico, and Virgin Islands). Remarkably, the cumulative ILI+ for influenza A/H1 in region 2 during this 10-week period is over three times the expected value without NPIs. This is potentially an artifact due to the elevated medical visits among patients with ILI during this period (Fig. 1B). The New York area was the epicenter of the COVID-19 pandemic during the spring 2020 wave. Driven by the concern about infection, patients with ILI symptoms, many of which overlap with COVID-19 symptoms (e.g., fever and cough), appear to have flooded into hospitals to seek medical treatments, resulting in a sharp spike of ILI in March and April 2020 (Fig. 1B). During this period, however, the positivity rate of A/H1 remained at levels similar to the period before the announcement of control measures. The increased probability of healthcare-seeking among patients with ILI likely contributed to the increase of ILI+ and is the primary factor that introduces bias into the ILI+ signal in region 2. Similar elevations of ILI in late March and early April also appeared in other regions, but with less pronounced effect. We conclude that the ILI+ data in

region 2 are biased due to changing healthcare-seeking behavior. A similar anomaly is also observed for influenza B in region 2. As the temporal variation of healthcare-seeking behavior cannot be precisely estimated, it is challenging to correct this bias in the ILI data. We therefore omitted the biased results for region 2 from Fig. 4. Influenza B activity was reduced by 67.3% to 91.3% in regions 3-9; however, the reduction is much lower in region 1 and region 10.

We further estimated the reduction of transmission rate for Influenza A/H1 and B after the implementation of NPIs. Specifically, we introduced a multiplier $\theta \in [0,1]$ to represent the percentage reduction of R_{0max} and R_{0min} caused by NPIs. We then fixed the model parameters R_{0max}, R_{0min}, D and L at the values estimated before the enforcement of NPIs and ran MCMC simulations to obtain the optimal value of θ that best fits the ILI+ data after March 15, 2020. The estimated percentage reduction parameters θ for the US and HHS regions (except region 2) are provided in Table 1.

Long-term effect

To investigate the potential impact of NPIs on the future dynamics of influenza, we projected influenza transmission at the national scale over the next five years using the humidity-driven SIRS model under two different control scenarios. For the two scenarios, we assume that current control efforts last 1.5 and 2 years after March 15, 2020, respectively. During the control period, the maximum and minimum daily basic reproductive numbers (R_{0max} and R_{0min}) were reduced by 55%, per the estimated reduction of transmission rate for Influenza A/H1 in the US. Once NPIs are relaxed, R_{0max} and R_{0min} resume to the values estimated from data before the pandemic. Due to waning immunity and immune escape attributed to antigenic drift, population susceptibility to each type of influenza accumulates over time. As antigenic drift is punctuated and not necessarily gradual, it is challenging to predict the rate of

immunity loss. To this end, we tested three hypothetical rates of susceptibility accumulation by assuming a mean duration of immunity of 2, 3 or 4 years, respectively.

Projections indicate that, for both influenza A/H1 and B, transmission is fully suppressed during the control period, as has been observed for the 2020-2021 season (Fig. 5). After control is relaxed, a large-scale outbreak occurs due to the accumulation of susceptible individuals. A longer control period leads to a larger susceptible population that supports a higher epidemic peak. Subsequent transmission dynamics are an interplay between humidity-forced seasonality and population susceptibility, resulting in distinct peak timing within different seasons. For each choice of immunity duration, epidemic size decreases following the first large-scale outbreak, and gradually returns to pre-pandemic levels. Under both control scenarios, a shorter immunity duration leads to an earlier epidemic onset. The magnitude of epidemic peak intensity decreases with increasing duration of immunity, so does the frequency of outbreaks over the next five years. According to the projections, the downstream, ripple-effects of pandemic NPIs could persist for a number of years.

Discussion

Both influenza A/H1 and B showed significant reductions of incidence in the US after implementation of NPIs for COVID-19 control during the 2019-2020 season. In the short term, the control measures are expected to decrease the number of influenza infections and alleviate the burden on healthcare systems. However, after the NPIs are relaxed, the potential accumulation of susceptibility to influenza infection may lead to a large outbreak. Healthcare systems need to prepare for potential patient surges and advocate vaccination and continued precautions, especially among high-risk population. High influenza vaccination uptake will be important for the prevention of large-scale post-pandemic surge of influenza. However, due to the global suppression of influenza activity during the COVID-19 pandemic, it may be

difficult to predict future circulating strains to inform the production of influenza vaccines. As a result, vaccine effectiveness might be reduced.

Influenza A/H1 and B were prevalent in the US during the 2019-2020 season, thus we focused on these two types/subtypes. However, circulating types/subtypes may differ each year and it is challenging to predict which ones will dominate in the coming years. As the transmission of all influenza types/subtypes was suppressed under NPIs, it is possible the incidence of all types/subtypes could surge within a single season, together with other respiratory infections. Specifically, A/H3 has not been prevalent in the US for two consecutive seasons (2019-2020 and 2020-2021). The next outbreak of A/H3 is particularly worrisome due to its relatively higher mortality rate [32]. For instance, influenza A/H3 predominated overall during the 2017-2018 season and led to the highest influenza-related mortality since 2010 [32]. Further, ILI-related patient visits are attributed to a number of respiratory diseases [34]; simultaneous surges of patients infected with different respiratory viruses within one season could substantially strain resources in healthcare systems.

Several limitations need to be noted regarding the results. The reported influenza incidence in the 2019-2020 season could be biased. The increased ILI-related visits in March and April of 2020 due to people's concern for the SARS-CoV-2 infection were observed in almost all regions, and particularly pronounced in region 2. However, after the initial phase, people tended to stay at home, only go out for essential services, and avoid visiting hospitals unless necessary. The reported patients with ILI symptoms during this period could thus be underestimated.

Apart from NPIs, the dynamics of influenza may be affected by direct interaction with SARS-CoV-2. Pre-existing immunity to SARS-CoV-2 was observed in people never exposed to this virus, and T cell memory to 'common cold' coronaviruses may account for this

phenomenon [35]. The interactions between co-circulating pathogens may bring interlinked epidemiological patterns of infection, and these interactions among respiratory viruses have been reported in a previous study [36]. Thus, it is possible that broad-acting immunity may be associated with the decrease in influenza infection.

Lastly, the accumulation of population susceptibility to influenza is presumed to be a function of waning immunity and antigenic escape. If antigenic escape is the predominant mechanism, then the accrual of population susceptibility to influenza may be very reduced, as antigenic advance depends on serial passage in the general population, which is currently suppressed. If this is so, influenza may simply return to prior activity levels once NPIs are relaxed.

Reference

1. World Health Organization. Coronavirus disease (COVID-19). Available at: https://www.who.int/emergencies/diseases/novel-coronavirus-2019. Accessed April 19, 2021.

2. Centers for Disease Control and Prevention. COVID Data Tracker. Available at: https://covid.cdc.gov/covid-data-tracker. Accessed April 19, 2021.

3. Chinazzi M, Davis JT, Ajelli M, et al. The effect of travel restrictions on the spread of the 2019 novel coronavirus (COVID-19) outbreak. Science **2020**; 368:395-400.

4. Pei S, Yamana TK, Kandula S, Galanti M, Shaman J. Burden and characteristics of COVID-19 in the United States during 2020. Nature **2021;** https://doi.org/10.1038/s41586-021-03914-4.

5. World Health Organization. Report of the WHO-China Joint Mission on Coronavirus Disease 2019 (COVID-19). Available at: https://www.who.int/publications-detail-redirect/report-of-the-who-china-joint-mission-on-coronavirus-disease-2019-(covid-19). Accessed May 7, 2021.

6. Viner RM, Russell SJ, Croker H, et al. School closure and management practices during coronavirus outbreaks including COVID-19: a rapid systematic review. Lancet Child Adolesc Health **2020**; 4:397-404.

7. Pei S, Kandula S, Shaman J. Differential effects of intervention timing on COVID-19 spread in the United States. Sci Adv **2020**; 6: eabd6370.

8. Tian H, Liu Y, Li Y, et al. An investigation of transmission control measures during the first 50 days of the COVID-19 epidemic in China. Science **2020**; 368:638-42.

9. Baker RE, Park SW, Yang W, Vecchi GA, Metcalf CJE, Grenfell BT. The impact of COVID-19 nonpharmaceutical interventions on the future dynamics of endemic infections. Proc Natl Acad Sci U S A **2020**; 117:30547-53.

10. Lei H, Xu M, Wang X, et al. Nonpharmaceutical Interventions Used to Control COVID-19 Reduced Seasonal Influenza Transmission in China. J Infect Dis **2020**; 222:1780-3.

11. Cowling BJ, Ali ST, Ng TWY, et al. Impact assessment of non-pharmaceutical interventions against coronavirus disease 2019 and influenza in Hong Kong: an observational study. Lancet Public Health **2020**; 5:e279-e88.

12. Zipfel CM, Colizza V, Bansal S. Double trouble? When a pandemic and seasonal virus collide. medRxiv **2021**; doi: https://doi.org/10.1101/2020.03.30.20047993.

13. Leung NHL, Chu DKW, Shiu EYC, et al. Respiratory virus shedding in exhaled breath and efficacy of face masks. Nat Med **2020**; 26:676-80.

14. Soo RJJ, Chiew CJ, Ma S, Pung R, Lee V. Decreased Influenza Incidence under COVID-19 Control Measures, Singapore. Emerg Infect Dis **2020**; 26:1933-5.

15. Lim JT, Chew LZX, Choo ELW, et al. Increased Dengue Transmissions in Singapore Attributable to SARS-CoV-2 Social Distancing Measures. J Infect Dis **2021**; 223:399-402.

16. Cavany SM, España G, Vazquez-Prokopec GM, Scott TW, Perkins TA. The impacts of COVID-19 mitigation on dengue virus transmission: a modelling study. medRxiv **2021**; doi: https://doi.org/10.1101/2020.11.17.20210211.

17. Park SW, Pons-Salort M, Messacar K, et al. Epidemiological dynamics of enterovirus

D68 in the United States and implications for acute flaccid myelitis. Sci Transl Med **2021**; 13: eabd2400.

18. Molinari N-AM, Ortega-Sanchez IR, Messonnier ML, et al. The annual impact of seasonal influenza in the US: measuring disease burden and costs. Vaccine **2007**; 25:5086-96.

19. Brankston G, Gitterman L, Hirji Z, Lemieux C, Gardam M. Transmission of influenza A in human beings. Lancet Infect Dis **2007**; 7:257-65.

20. Killingley B, Nguyen-Van-Tam J. Routes of influenza transmission. Influenza Other Respir Viruses **2013**; 7 Suppl 2:42-51.

21. Lei H, Li Y, Xiao S, et al. Routes of transmission of influenza A H1N1, SARS CoV, and norovirus in air cabin: Comparative analyses. Indoor Air **2018**; 28:394-403.

22. Centers for Disease Control and Prevention. National, Regional, and State Level Outpatient Illness and Viral Surveillance. Available at: https://gis.cdc.gov/grasp/fluview/fluportaldashboard.html. Accessed April 20, 2021.

23. Shaman J, Karspeck A, Yang W, Tamerius J, Lipsitch M. Real-time influenza forecasts during the 2012-2013 season. Nat Commun **2013**; 4:2837.

24. Shaman J, Kohn M. Absolute humidity modulates influenza survival, transmission, and seasonality. Proc Natl Acad Sci U S A **2009**; 106:3243-8.

25. Cosgrove BA, Lohmann D, Mitchell KE, et al. Real- time and retrospective forcing in the North American Land Data Assimilation System (NLDAS) project. J Geophys Res **2003**; 108:2002JD003118.

26. Shaman J, Karspeck A. Forecasting seasonal outbreaks of influenza. Proc Natl Acad Sci U S A **2012**; 109:20425-30.

27. Pei S, Kandula S, Yang W, Shaman J. Forecasting the spatial transmission of influenza in the United States. Proc Natl Acad Sci U S A **2018**; 115:2752-7.

28. Pei S, Shaman J. Counteracting structural errors in ensemble forecast of influenza outbreaks. Nat Commun **2017**; 8:925.

29. Pei S, Teng X, Lewis P, Shaman J. Optimizing respiratory virus surveillance networks using uncertainty propagation. Nat Commun **2021;** 12:222.

30. Shaman J, Pitzer V, Viboud C, Lipsitch M, Grenfell B. Absolute Humidity and the Seasonal Onset of Influenza in the Continental US. PLoS Curr **2009**; 2:RRN1138.

31. Chib S, Greenberg E. Understanding the Metropolis-Hastings Algorithm. Am Stat **1995**; 49:327.

32. Centers for Disease Control and Prevention. Disease Burden of Influenza. Available at: https://www.cdc.gov/flu/about/burden/index.html. Accessed April 5, 2021.

33. RDocumentation. forecast package - RDocumentation. Available at: https://www.rdocumentation.org/packages/forecast/versions/8.14. Accessed April 20, 2021.

34. Pei S, Shaman J. Aggregating forecasts of multiple respiratory pathogens supports more accurate forecasting of influenza-like illness. PLoS Comput Biol **2020**; 16:e1008301.

35. Sette A, Crotty S. Pre-existing immunity to SARS-CoV-2: the knowns and unknowns. Nat Rev Immunol **2020**; 20:457-8.

36. Nickbakhsh S, Mair C, Matthews L, et al. Virus-virus interactions impact the population dynamics of influenza and the common cold. Proc Natl Acad Sci U S A **2019**; 116:27142-50.

Fig 1. Influenza activity during past seasons. (A) Weekly ILI (percentage) at national level during the 2011-2012 to 2019-2020 seasons. Week 1 in the x-axis is the 40th week in each year. (B) ILI+ (incidence per 100,000 people) for influenza A/H1 and B in the US during the 2019-2020 season. (C-D) ILI+ (incidence per 100,000 people) for influenza A/H1 and B for the 10 HHS regions during the 2019-2020 season.

Fig 2. Examples of retrospective forecasts at the national level. (A) Influenza A/H1 in the US during the 2018-2019 season. Green dots are observed weekly ILI+ (incidence per 100,000 people). The vertical dash line indicates the forecast week. Grey line is the mean model fitting (before the forecast week) and mean prediction (after the forecast week), and the grey shaded area shows the 95% CI (credible interval). (B) Influenza A/H1 in the US during the 2015-2016 season. (C) Influenza B in the US during the 2017-2018 season. (D) Influenza B in the US during the 2012-2013 season. The unit of ILI+ is incidence per 100,000 people.

Fig 3. Fitted and predicted curves at the national level in the 2019-2020 season. Green dots are observed weekly ILI+ (incidence per 100,000 people). Vertical dotted lines indicate the forecast week (week 24). Grey lines are the mean model fitting (before the forecast week) and mean prediction (after the forecast week). The grey shaded area shows the 95% CI (credible interval).

Fig 4. Reduction of influenza activity in 10 HHS regions within 10 weeks after March 15th, 2020. Results are shown for influenza A/H1 (A) and B (B). The result for region 2 is omitted due to abnormal data reporting.

Fig 5. Simulated influenza activity in five years after 2020. The projected activity of influenza A/H1 under 1.5 years (A) and 2 years of NPIs (B) is shown. Projections for influenza B under 1.5 years and 2 years of NPIs are shown in (C) and (D). The average duration of immunity is assumed to be 2, 3 and 4 years. The vertical dash lines indicate the time point of relaxation of NPIs. The unit of ILI+ is incidence per 100,000 people.

Table 1. Reduction of transmission rates in US and 10 HHS regions within 10 weeks after March 15, 2020 (week 24). Results for region 2 are omitted due to irregular ILI reporting.

Region	A/H1	B
US	55%	33%
1	65%	26%
2	NA	NA
3	81%	52%
4	66%	53%
5	64%	30%
6	85%	61%
7	78%	88%
8	63%	33%
9	53%	27%
10	59%	92%

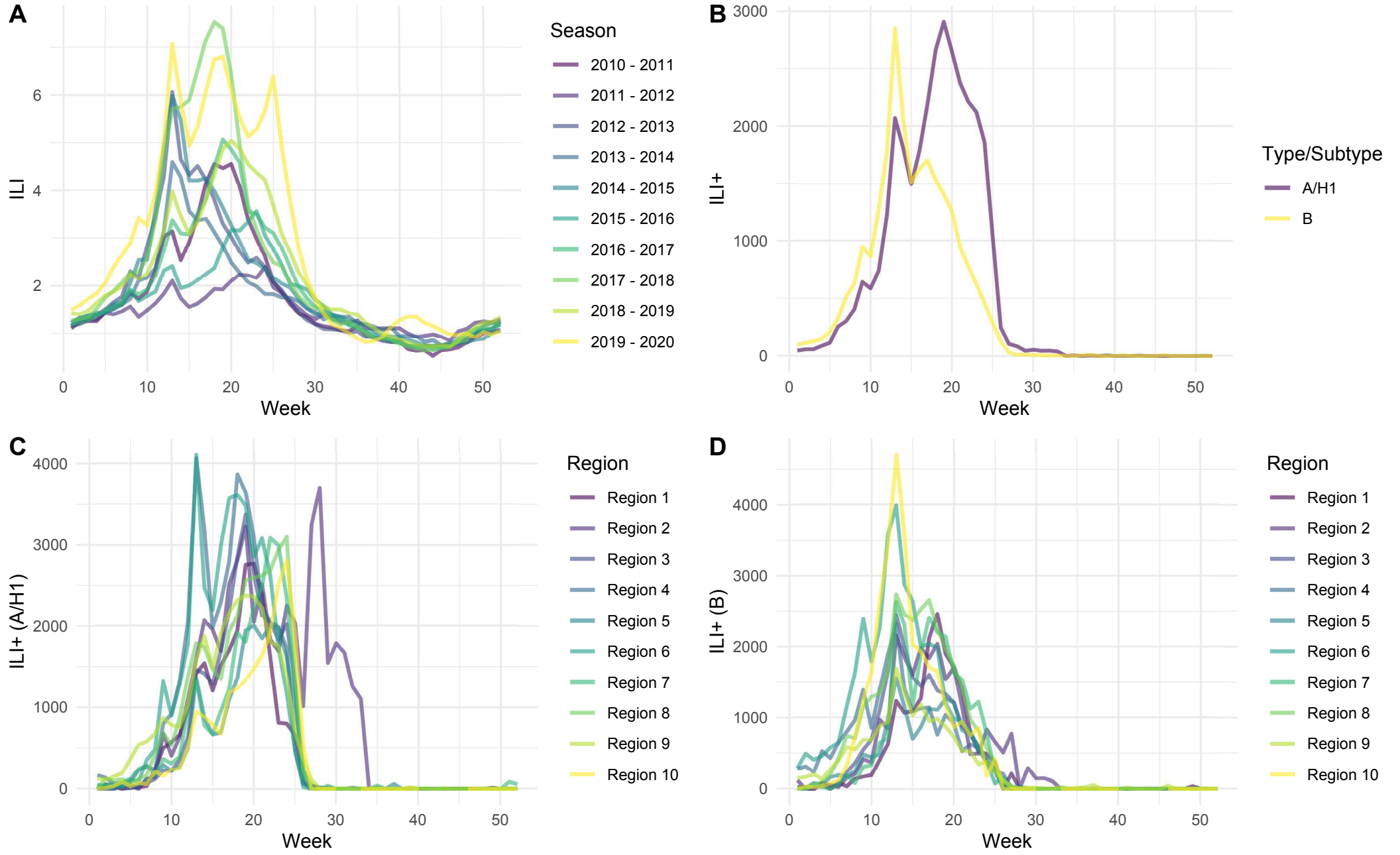
A
ILI
Week
Season
2010 - 2011
2011 - 2012
2012 - 2013
2013 - 2014
2014 - 2015
2015 - 2016
2016 - 2017
2017 - 2018
2018 - 2019
2019 - 2020
B
ILI+
Week
Type/Subtype
A/H1
B
C
ILI+ (A/H1)
Week
Region
Region 1
Region 2
Region 3
Region 4
Region 5
Region 6
Region 7
Region 8
Region 9
Region 10
D
ILI+ (B)
Week
Region
Region 1
Region 2
Region 3
Region 4
Region 5
Region 6
Region 7
Region 8
Region 9
Region 10

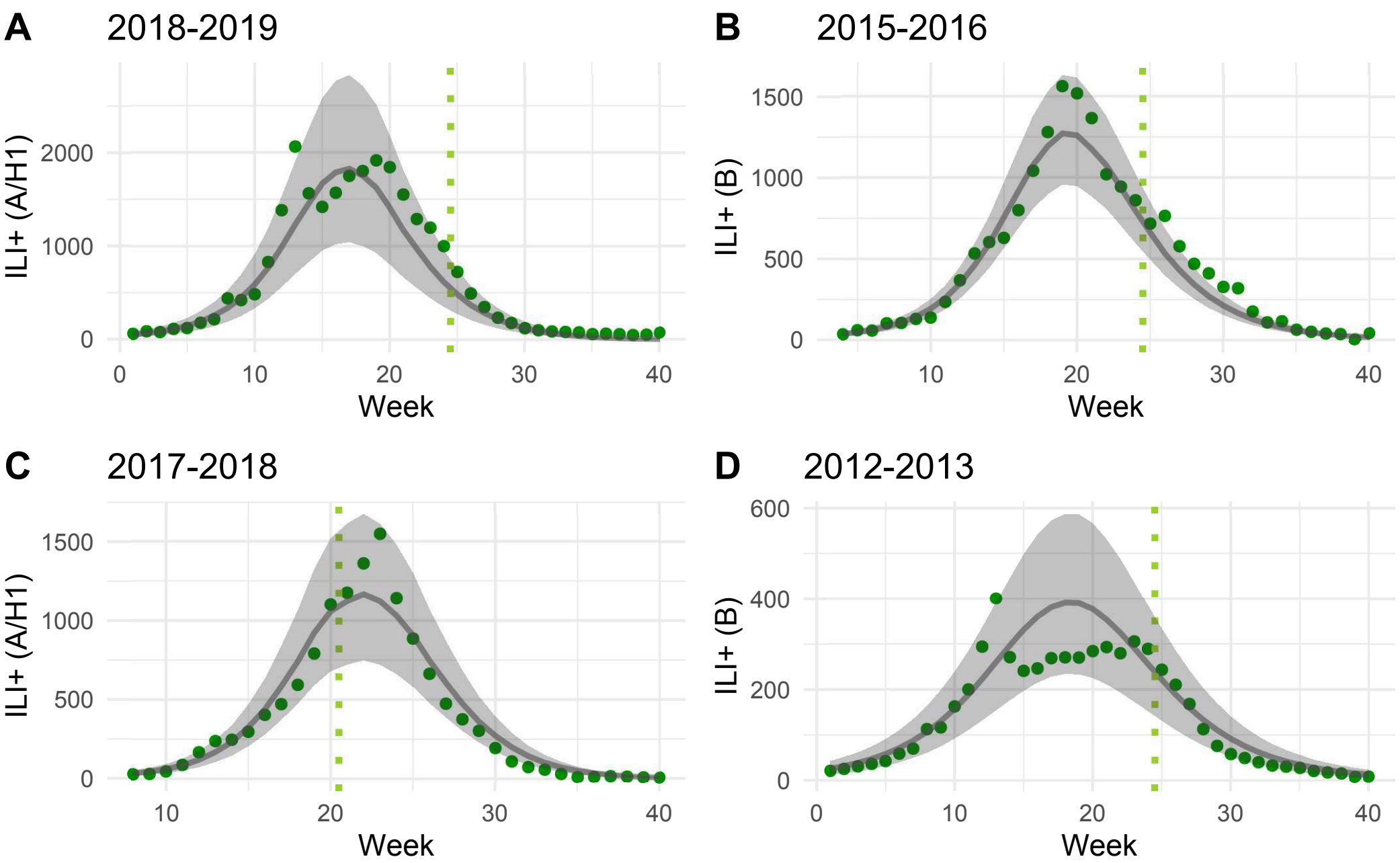
A
2018-2019
ILI+ (A/H1)
2000
1000
0
0
10
20
30
40
Week
B
2015-2016
ILI+ (B)
1500
1000
500
0
10
20
30
40
Week
C
2017-2018
ILI+ (A/H1)
1500
1000
500
0
10
20
30
40
Week
D
2012-2013
ILI+ (B)
600
400
200
0
0
10
20
30
40
Week

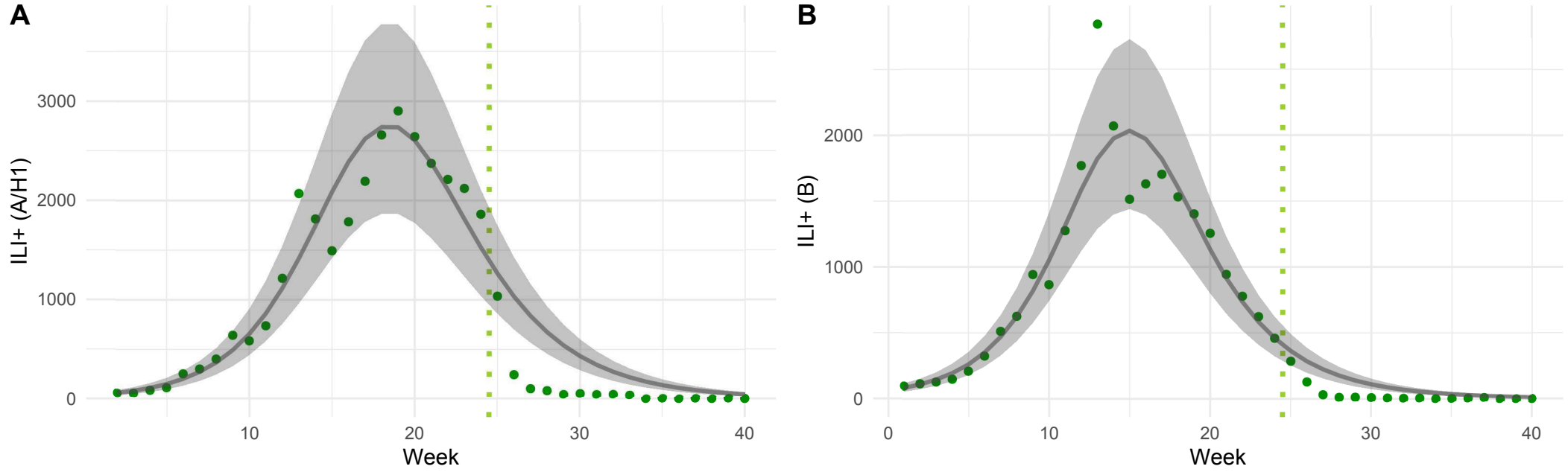
A
ILI+ (A/H1)
3000
2000
1000
0
10
20
30
40
Week
B
ILI+ (B)
2000
1000
0
0
10
20
30
40
Week

A

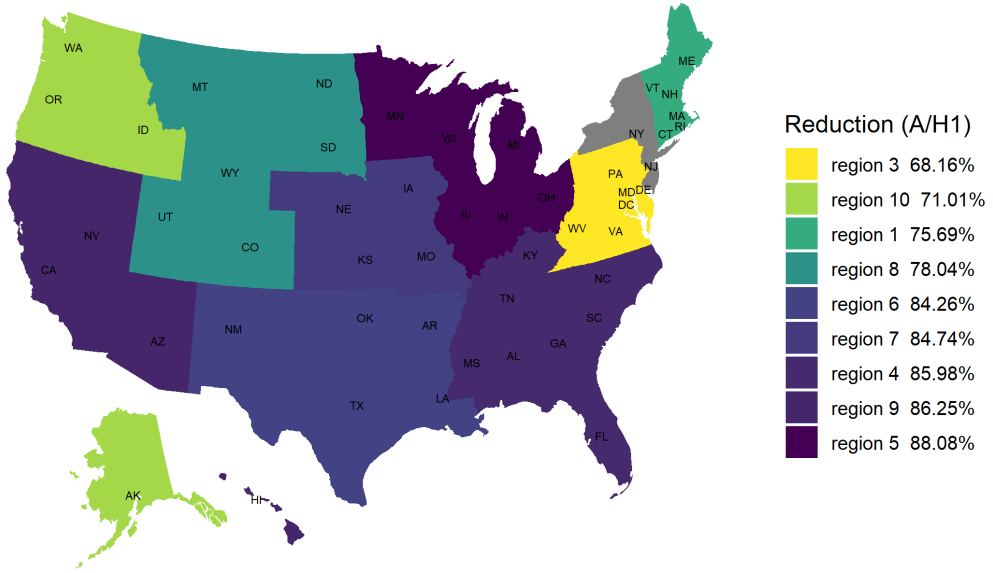

Reduction (A/H1)

- region 3 68.16%
- region 10 71.01%
- region 1 75.69%
- region 8 78.04%
- region 6 84.26%
- region 7 84.74%
- region 4 85.98%
- region 9 86.25%
- region 5 88.08%

B

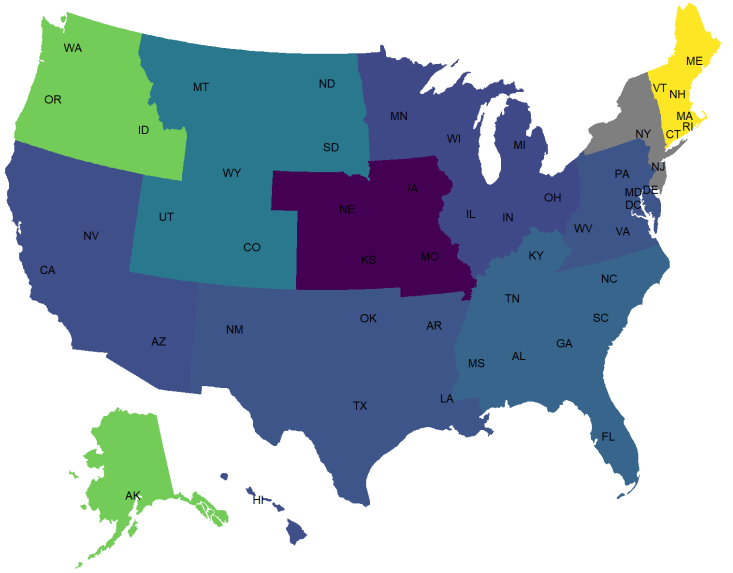

Reduction (B)

- region 1 31.5%
- region 10 44.8%
- region 8 67.3%
- region 4 71.9%
- region 3 75.4%
- region 6 75.5%
- region 9 76.9%
- region 5 78.3%
- region 7 91.3%

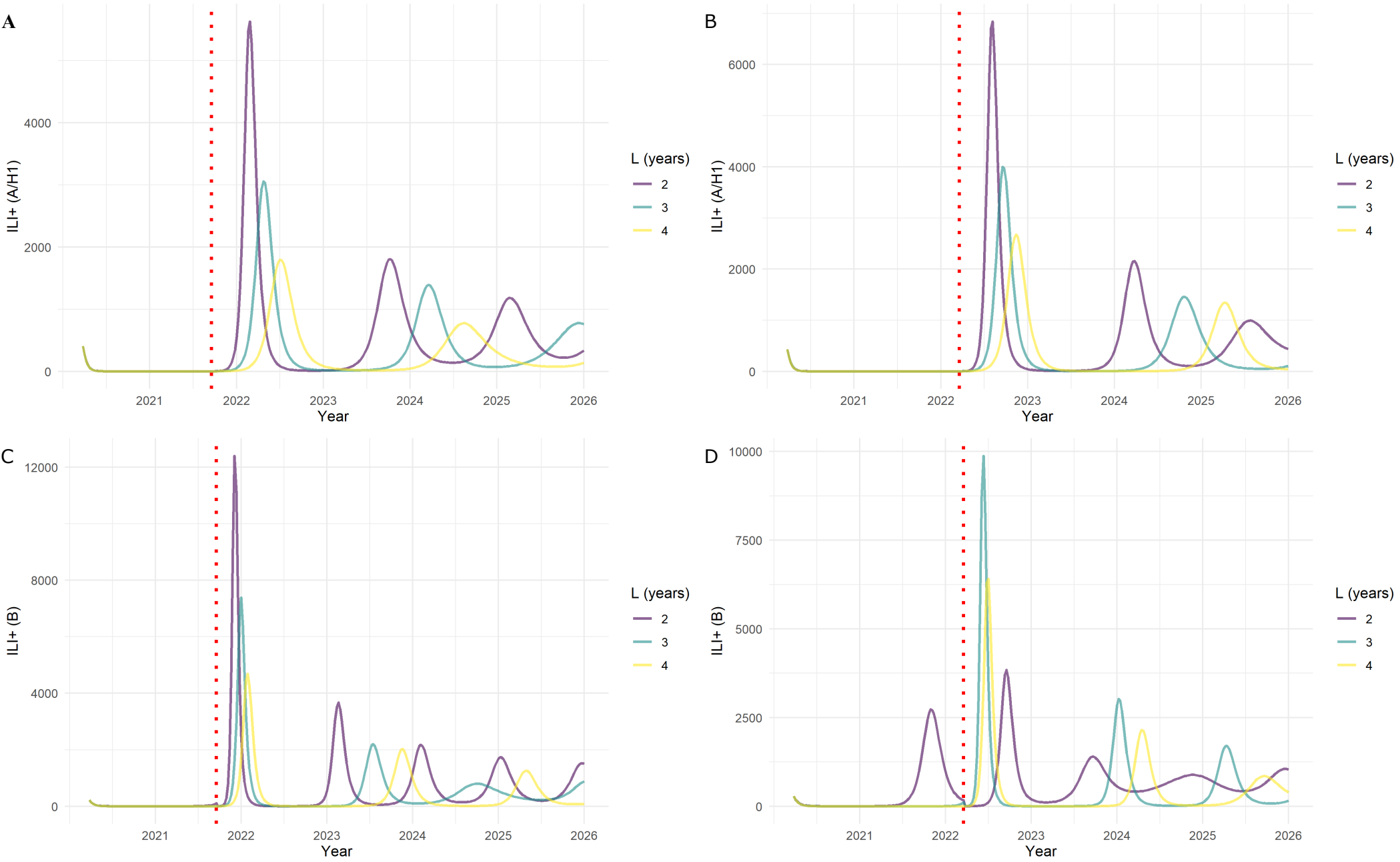
A
B
C
D
ILI+ (A/H1)
ILI+ (B)
Year
L (years)
2
3
4
0
2000
4000
6000
8000
10000
12000
2500
5000
7500
2021
2022
2023
2024
2025
2026